LASER & PHOTONICS REVIEWS
www.lpr-journal.org

Induced Photon Correlations Through the Overlap of Two Four-Wave Mixing Processes in Integrated Cavities

Yanbing Zhang, Michael Kues, Piotr Roztocki, Christian Reimer, Bennet Fischer, Benjamin MacLellan, Arstan Bisianov, Ulf Peschel, Brent E. Little, Sai T. Chu, David J. Moss, Lucia Caspani, and Roberto Morandotti**

Induced photon correlations are directly demonstrated by exploring two coupled nonlinear processes in an integrated device. Using orthogonally polarized modes within an integrated microring cavity, phase matching of two different nonlinear four-wave mixing processes is achieved simultaneously, wherein both processes share one target frequency mode, while their other frequency modes differ. The overlap of these modes leads to the coupling of both nonlinear processes, producing photon correlations. The nature of this process is confirmed by means of time- and power-dependent photon correlation measurements. These findings are relevant to the fundamental understanding of spontaneous parametric effects as well as single-photon-induced processes, and their effect on optical quantum state generation and control.

Quantum correlations, where two or more parties exhibit strong relations in a particular degree of freedom, are important resources for fundamental science such as the exploration of nonlocality and entanglement, as well as related technologies including quantum computation,[1] secure key distribution,[2] and nonclassical metrology.[3] For photons, these correlations can be created in several degrees of freedom. Correlated photon pairs are typically obtained via spontaneous nonlinear processes, for example, by exploiting spontaneous parametric down conversion (SPDC) in $\chi^{(2)}$ media[4] or spontaneous four-wave mixing (SFMW) in $\chi^{(3)}$ platforms.[5–7] Beyond standard bidimensional variables' correlations, such as for polarization, numerous quantum states with large Hilbert spaces have been generated based on these spontaneous processes, such as multicorrelated states,[8–12] multiple photon,[1,13,14] high-dimensional entangled states,[15–18] hyperentangled systems,[18,19] as well as multiphoton high-dimensional states.[20,21] In addition to spontaneous processes, photon correlations can also be obtained via

Y. Zhang, P. Roztocki, C. Reimer, B. Fischer, B. MacLellan, R. Morandotti
Énergie Matériaux Télécommunications
Institut National de la Recherche Scientifique
1650 Boulevard Lionel-Boulet, Varennes, Québec J3X 1S2, Canada
E-mail: morandotti@emt.inrs.ca

M. Kues
Hannover Center for Optical Technologies
Leibniz University Hannover
Nienburger Str. 17, Hannover 30167, Germany
E-mail: michael.kues@hot.uni-hannover.de

M. Kues
Cluster of Excellence PhoenixD (Photonics, Optics, and Engineering–Innovation Across Disciplines)
Leibniz University Hannover
Hannover, Germany

C. Reimer
HyperLight Corporation
501 Massachusetts Avenue, Cambridge, MA 02139, USA

The ORCID identification number(s) for the author(s) of this article can be found under https://doi.org/10.1002/lpor.202000128

DOI: 10.1002/lpor.202000128

A. Bisianov, U. Peschel
Institute of Solid State Physics and Optics
Abbe Center of Photonics
Friedrich Schiller University Jena
Max-Wien-Platz 1, Jena 07743, Germany

B. E. Little
State Key Laboratory of Transient Optics and Photonic
Xi'an Institute of Optics and Precision Mechanics
Chinese Academy of Sciences
Xi'an 710119, China

S. T. Chu
Department of Physics
City University of Hong Kong
Tat Chee Avenue
Hong Kong, China

D. J. Moss
Centre for Micro Photonics
Swinburne University of Technology
Hawthorn, Victoria 3122, Australia

L. Caspani
Institute of Photonics
Department of Physics
University of Strathclyde
Glasgow G1 1RD, UK

R. Morandotti
Institute of Fundamental and Frontier Sciences
University of Electronic Science and Technology of China
Chengdu, Sichuan 610054, China

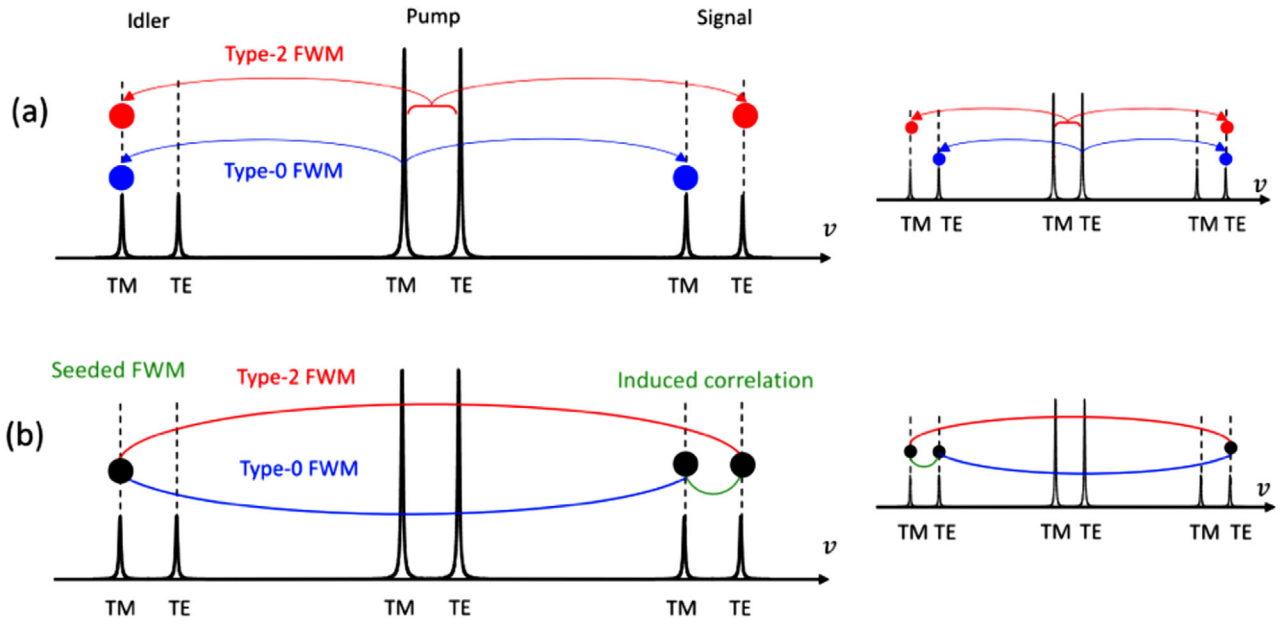

Figure 1. Working principle of the induced photon correlation process. a) Schematic of type-0 FWM (blue) on the TM left outer and an inner TM resonance together with type-2 FWM (red) on the outer TM and TE resonances of a cavity. The type-2 FWM process generates and correlates a TE signal photon and a TM idler photon, while the type-0 FWM process generates and correlates a TM signal photon and a TM idler photon (additionally, the type-0 FWM on the TE mode and the type-2 process on the outer TM and TE mode occur, as shown in the inset. Such processes introduce noise to the induced correlation). b) Sharing of a TM idler photon induces the correlation between a signal TM photon and a signal TE photon, resulting in induced correlation.

single-photon-seeded processes either mediated by stimulated emission[22] or in its absence.[23–25] The former has been very recently demonstrated in optical fibers by seeding single photons in a four-wave mixing (FWM) process,[22] and the latter has been reported in free-space $\chi^{(2)}$ nonlinear crystals.[23] So far, all single-photon-seeded processes required pregenerated single photons for the seeding process, and thus need either several crystals/paths or postprocessing.

Here, we demonstrate an induced photon correlation effect through a direct overlap of two distinct nonlinear processes in an integrated cavity. By exploiting the spatial multimode structure of an on-chip microring resonator, we were able to simultaneously phase-match two different SFWM processes (degenerate and nondegenerate) by exciting two orthogonally polarized modes (i.e. the transverse electric (TE) and transverse magnetic (TM) mode).[25] Since the two processes shared one of the frequency modes, a coupling of the two processes occurs, leading to an induced correlation between the two signal photons originating from distinct SFWM effects. We confirmed this induced correlation phenomenon with coincidence measurements, exploring the process dependence on the temporal and power characteristics of the excitation pulses.

We explore a novel type of induced correlation FWM process, which we term simply "seeded FWM" (see **Figure 1**). It takes place in a bichromatically pumped optical parametric oscillator involving both type-0 and type-2 FWM processes.[25–28] In the pump-degenerate type-0 process, two pump photons from the same TM polarized pump field are converted into two new photons (signal and idler), with the same polarization as the excitation field (see Figure 1a, blue lines). In the pump-nondegenerate type-2 process, on the other hand, the two annihilated photons, each originating from a different polarized pump field (TE and TM), produce an orthogonally polarized photon pair (see Figure 1a, red lines). More importantly, interference between the two FWM processes produces correlations. Because of the temporal and spatial overlaps and the single, shared resonance frequency, a single generated photon from either type-0 or type-2 FWM seeds the other nonlinear process, introducing coupling between the two processes. As for the example shown in Figure 1b, a TM idler photon induces correlation between the signal TM and TE photons. Such induced correlation is created indirectly (i.e., via two parametric processes that are linked).

The experiment was based on a 4-port integrated microring resonator fabricated on a high-refractive-index glass,[29–31] pigtailed with polarization-maintaining fibers at each port, featuring a coupling loss of 1.7 dB per facet. The measured spectral response of the microcavity at the drop port (see **Figure 2**) shows two orthogonally polarized modes with almost identical free spectral ranges around 200 GHz (200.4 GHz for TM and 200.5 GHz for TE). The insets depict the transmission of the three resonance pairs under investigation on a linear scale with a Lorentzian fit, demonstrating Q-factors of around 240 000 (TE mode) and 480 000 (TM mode), corresponding to resonance bandwidths of 820 and 410 MHz, respectively. In order to suppress the spurious stimulated FWM emission between the TE and TM modes and allow isolation between the type-0 and type-2 FWM processes, a frequency offset of 70 GHz between the two modes was engineered through a slightly different waveguide dispersion to locate the stimulated FWM gain outside of the cavity resonances.[25] The two modes exhibited small anomalous second-order dispersion over most of the C-band, and the zero dispersion wavelengths were measured to be at 1560 nm for the TE mode and 1595 nm for the TM mode,[29] respectively. At the same time, the TE and TM modes' dispersion had to be kept similar, in order to i) ensure

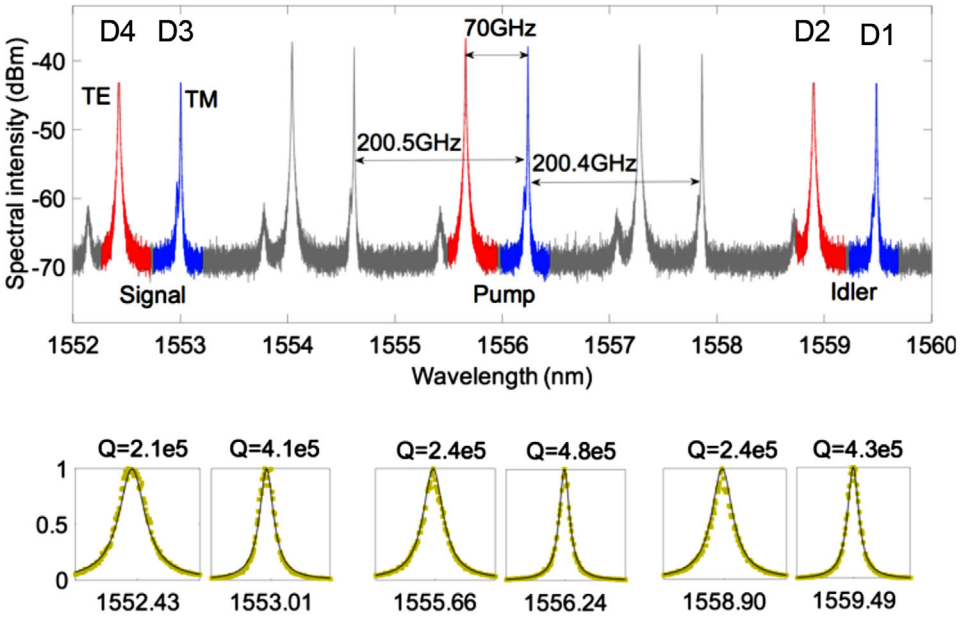

Figure 2. Microring resonator characteristics. Transmitted spectrum for a broadband input field (amplified spontaneous emission from an erbium-doped fiber amplifier (EDFA)) measured at the cavity drop port showing TE resonance modes separated by an FSR of 200.4 GHz and TM resonance modes separated by an FSR of 200.5 GHz with a relative frequency offset of 70 GHz. The experimentally chosen six resonances are highlighted, where the TE and TM modes are in red and blue, respectively. The insets below the transmission spectrum show the resonances in a linear scale (yellow marker) fitted with a Lorentzian shape (black solid line), alongside their corresponding total Q factors. The x-axis value indicates the center wavelength of each resonance in nanometers.

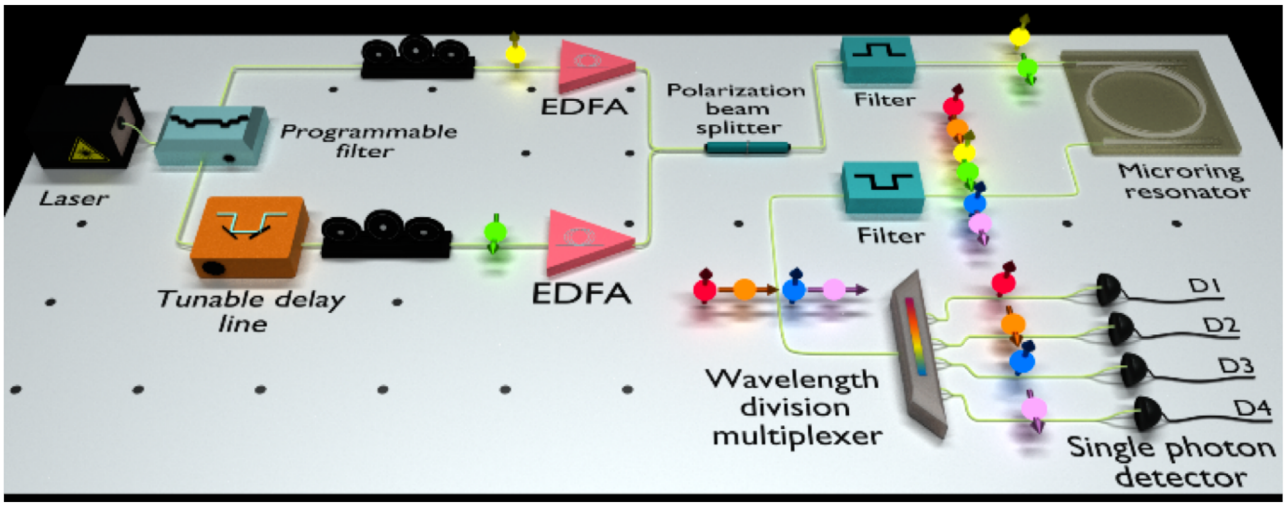

Figure 3. Experimental setup for single-photon-stimulated correlation. The two polarized pump modes were spectrally sliced from a 10 MHz mode-locked laser by a programmable optical filter, subsequently routed into different spatial modes and amplified individually by erbium-doped fiber amplifiers (EDFAs). A polarization beam splitter combined the two pump modes, being followed by a high-isolation band-pass filter before the tailored light field entered the microring resonator. The generated photons were guided to four single-photon detectors via a wavelength division multiplexer. The colored spheres with arrows illustrate the frequency and polarization of the involved fields: yellow and green indicate the TE and TM excitation fields, respectively, while red, orange, blue, and purple depict the generated photons. The total loss from the drop port of the microring to the detector was ≈5 dB.

that the difference in free spectral range between the two orthogonally polarized modes (120 MHz) was smaller than the minimum bandwidth of the resonances (410 MHz), and to ii) satisfy energy conservation for the type-2 FWM process.[25]

We operated the microring resonator below the optical parametric oscillation threshold to observe single-photon-seeded FWM. To do this, we simultaneously excited the ring resonator with two orthogonally polarized pump modes (see **Figure 3** for details). A tunable delay line inserted in one pump path was used to tune and adjust the temporal overlap between the two excitation fields, allowing us to isolate the photon pair generation of the type-0 and type-2 processes. In order to achieve the

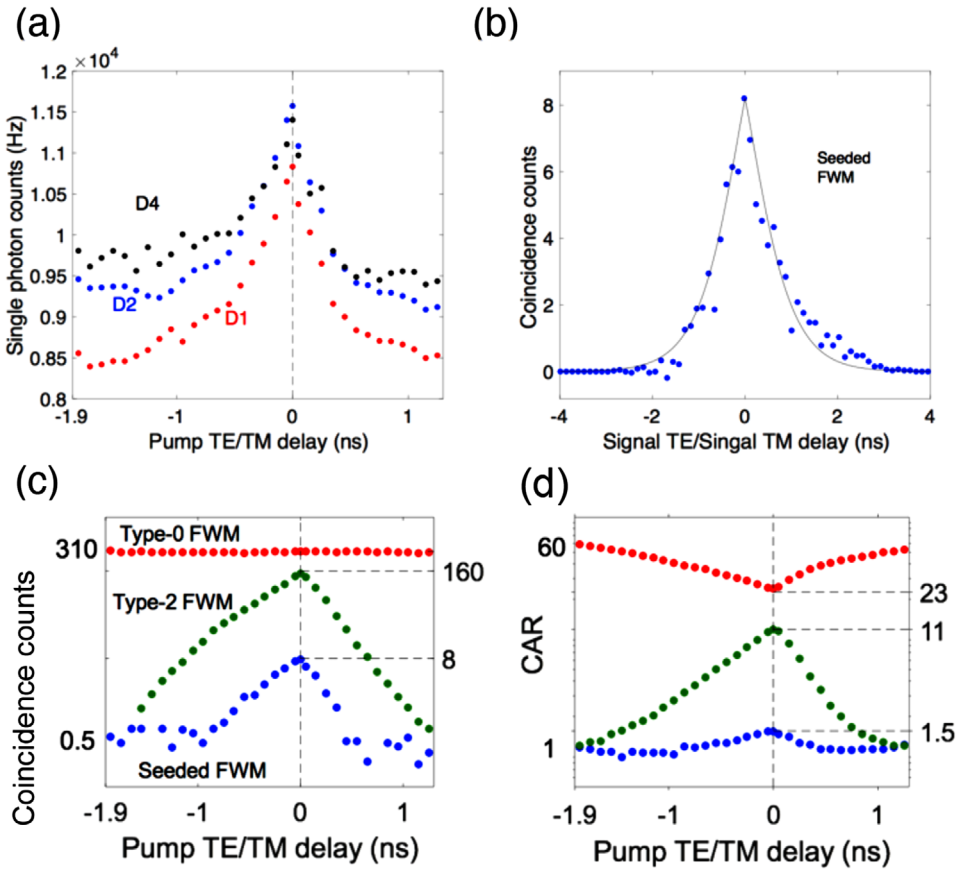

Figure 4. Effect of the temporal overlap of the pump TE and TM fields on spontaneous photon generation. a) Single photon counts in the individual channels. b) Measured photon coincidence peak between the TE and TM signal photons of the seeded FWM with background subtraction. The experimental data (dot) fit by a Glauber function[33] correspond to a measured photon bandwidth of 330 MHz, in line with the expected bandwidth of 410 MHz once the additional effect of the electronics and detectors time jitters was taken in consideration. c) Measured true photon coincidence counts (in 30 min) of type-0 FWM (D3–D1), type-2 FWM (D4–D1), and seeded FWM (D1–D2) in log scale as a function of the temporal overlap between the TE and TM pumps (adjusted through the tunable delay line). The dashed line indicates zero delay. d) Coincidence to accidental ratio (CAR) corresponding to panel (c) as a function of the TE/TM pump delay. The TE pump power was set to 110 μW and the TM pump to 440 μW.

FWM phase-matching condition, the microring resonator was excited at two adjacent TE and TM resonances (see Figure 2), located at 1555.65 and 1556.24 nm and featuring group velocity dispersion values of −1.3 and −9.2 ps^2 km^{-1}, respectively. To avoid spontaneous Raman noise, which is spectrally shifted in wavelength from the pump frequency to the red by around 6 nm,[14] the two TE/TM photon pair resonances were chosen to be at 1552.43 nm (TE signal, D4), 1553.01 nm (TM signal, D3), 1558.90 nm (TE idler, D2), and 1559.49 nm (TM idler, D1), and measured by detectors D1, D2, D3, and D4, respectively (see Figure 2). For a pulsed pump, the count of the generated photons scales with the product of the power of each pump (P_1 and P_2) and the squared cavity factor,[32] i.e., $\propto P_1 P_2 Q^2$. In order to compensate for different Q-factors and to ensure that the TE and TM modes generate a similar amount of photon counts, we set the TM and TE pump powers to 110 and 440 μW, respectively. To confirm photon generation and induced photon correlation FWM, we performed photon coincidence measurements for varying temporal overlap and power ratio of the pump fields.

To ensure that the induced photon correlation effect arose solely from the interaction between the type-0 and type-2 processes, we first investigated the effect of varying the temporal overlap between the TE and TM pump pulses. We selected photons from detectors D1, D3, and D4 for analysis. We saw that the single photon counts in each channel increased with reduced TE/TM pump delay (larger temporal overlap)—due to the improved efficiency in the type-2 SFWM process (see **Figure 4**a). However, we observed a completely different behavior for the type-0 FWM (TM signal and TM idler), type-2 FWM (TE signal and TM idler), and seeded FWM (TM signal and TE signal) processes, in terms of a true coincidence rate (C) and coincidence-to-accidental ratio (CAR). Specifically, when the two pump fields did not overlap in the temporal domain, only the type-0 FWM process occurred, confirmed by a constant high coincidence rate (D1–D3) of 310 Hz that was basically independent of the temporal delay (see Figure 4c). In contrast, the coincidence counts of the type-2 (D1–D4) and induced (D3–D4) correlation processes grew gradually with a reduced delay, and reached maximum values of 160 and 8 Hz, respectively, at zero delay. We measured a clear coincidence peak between the TM and TE signal photons at zero delay (see Figure 4b). This led to a coincidence rate ratio between the seeded and type-2 processes of 5%. In addition, the

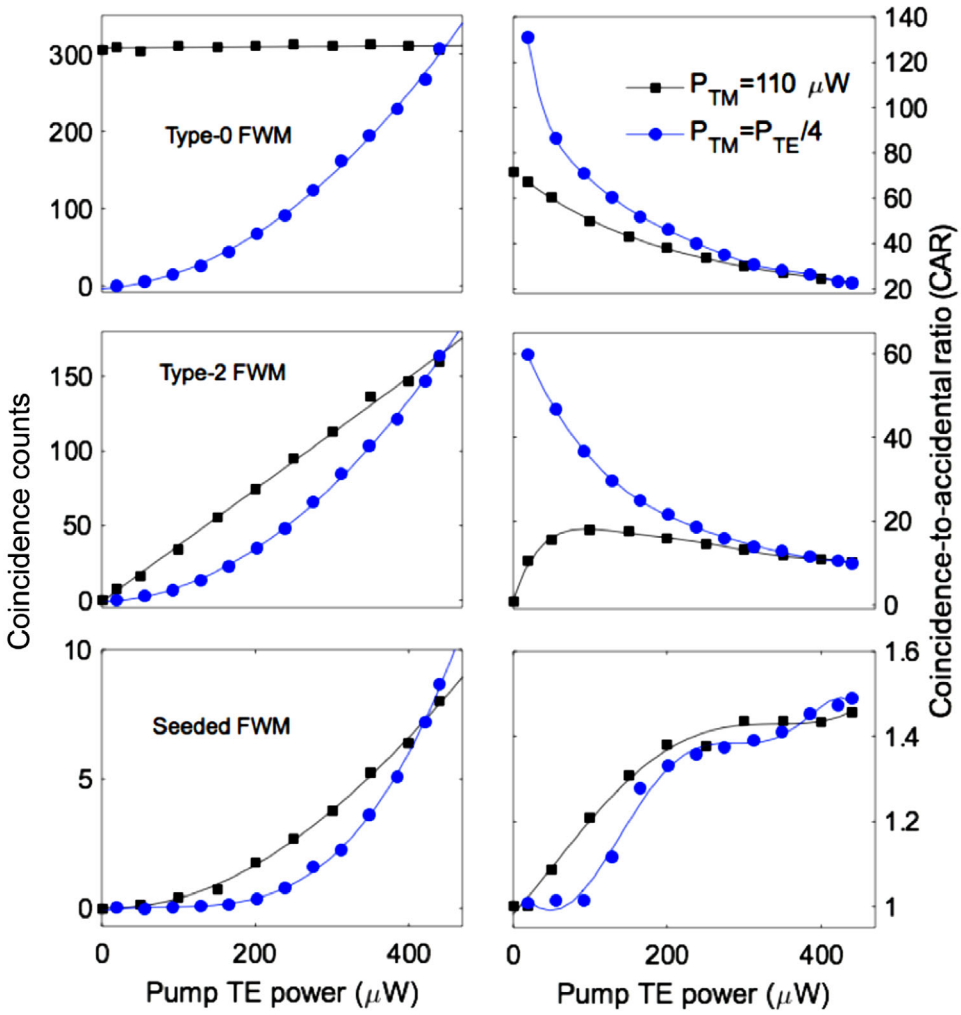

Figure 5. Power-dependent photon pair characterization. Coincidence counts acquired in 30 min (left) and CAR (right) as a function of the TE pump power for a fixed value of the TM pump power (P_{TM} = 110 μW, black squares) and of the power ratio ($P_{TM} = P_{TE}/4$, blue circles). In the left panels, the coincidence rates of the type-0, type-2, and seeded FWM (top to bottom) show a constant, linear, and quadratic behavior, respectively, for P_{TM} = 110 μW (black), while they show quadratic, quadratic, and quartic behavior, respectively, for power scaling when $P_{TM} = P_{TE}/4$. In the right panels, the lines connecting the points are for visual purposes.

same slope of the curves of type-2 and seeded FWM in Figure 4c yielded a constant ratio when varying the delay from −1 to 0.5 ns. This constant ratio, as well as the coincidence peak (Figure 4b), strongly confirms the existence of the induced photon correlation process, which was stimulated by the interplay between the type-0 and type-2 processes. Note that such a correlation cannot occur from two different type-2 processes, as their modes are not linked together. This situation can also be compared to two independent type-0 processes radiating into different signal and idler modes, where a correlation between two signal or two idler modes is not observed. Our finding was further supported by the CAR measurement (see Figure 4d), where the CARs of both seeded and type-2 FWM increased to their maxima of 1.5 and 11, respectively, at zero delay. In contrast, the CAR of type-0 FWM decreased from 60 to its minimum of 22, despite both pump power and photon coincidence remained constant. This is because the photons generated by the type-2 process are seen as noise photons by the type-0 process.

The induced photon correlation had a very low CAR. This is because the induced correlation is a nonquantum correlation. Due to the thermal characteristics of a single FWM process, the generated photons have super-Poissonian statistics. The photons from such a thermal process are then used to seed a second process that has also intrinsic thermal characteristics. In turn, the photons resulting from the seeded process are also super-Poissonian, and the CAR of the induced correlation will never reach a value larger than 2 (due to the Cauchy–Schwarz inequality). In other words, this observation can be understood as a conventional Hanbury–Brown–Twiss (HBT) measurement[34] of the TM idler resonance, but in the frequency domain. Unlike the conventional HBT setup, where a signal mode is split into two outputs with a 50:50 spatial beam splitter, here the TM idler photon is correlated

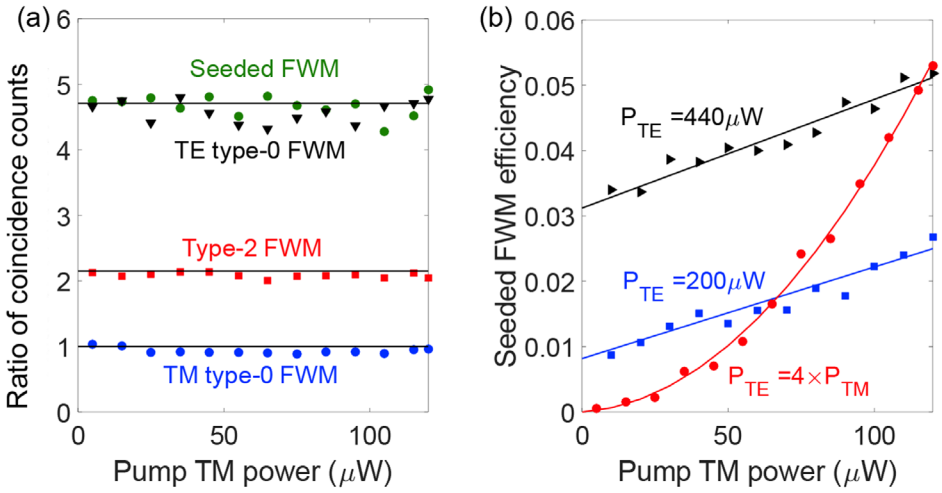

Figure 6. Induced correlation characterization as a function of power. a) Ratio of the measured true coincidence rates between processes with two different TE pump powers of 440 and 200 μW, $C(P_{TE} = 440\ \mu W)/C(P_{TE} = 200\ \mu W)$, as a function of the TM pump power, for different types of FWM (spontaneous TM type-0, blue; spontaneous TE type-0, black; spontaneous type-2, red; and seeded, green). The solid lines represent the theoretical values, which are 2.2 = 440/200, 4.84 = 2.2^2, and 1, respectively. The values extracted from experimental results present good agreement with the theoretical values. b) Seeded FWM efficiency shows a linear behavior with the TM pump power when the TE pump power is constant ($P_{TE} = 440$ μW and $P_{TE} = 200$ μW). When both pump powers are increased with a fixed power ratio ($P_{TE} = 4 \times P_{TM}$), a clear quadratic scaling behavior is observed without any linear contribution.

with two signal TM and TE frequencies using the type-0 and type-2 FMW processes. A CAR value of 1.5 agrees with expectations from the conventional mode measurement. The spectral overlap of the TE and TM modes results in two effective modes, leading to a CAR = 1.5 using $1 + 1/N_{eff}$ with the effective mode number $N_{eff} = 2$.[17]

The asymmetry of the coincidence counts and CAR curves with respect to the zero delay in Figure 4 is due to the different exponential decay of the cavity resonance emission. Since the type-2 process requires a temporal overlap between the two pump fields, the delay dependence of the coincidence counts and CAR reflects the pumps' resonance temporal information (the pumps' spectra are filtered by the cavity resonances). In our experiment, we delayed the TE pump pulse (with a temporal width of 0.6 ns) with respect to the TM pulse (with a temporal width of 1.2 ns), where negative delay means that the high-Q TM pump pulse is temporally ahead of the low-Q TE pump pulse. Therefore, the temporal decay of the pump resonances was reflected in the asymmetry associated with the CAR and coincidence profiles. For negative delays, the latter reflects the decay of the TM pulse, while for positive delays, the former represents the decay of the TE pulse. The concept of using the photon properties to extract information about the pump pulse is very similar to ultrafast pulse characterization using pump–probe effects based on classical nonlinear processes, such as nonlinear absorption and phase modulation of a weak probe field induced by a strong field.[35,36]

The power-scaling behavior provides an insight into the different photon generation processes. **Figure 5** summarizes the true coincidence counts (C) and their CARs. In theory, the true coincidence count of the TM type-0 process is proportional to the square of the TM pump power ($C \propto P_{TM}^2$), and the type-2 process is proportional to the product of both pump powers ($C \propto P_{TE} P_{TM}$). A contribution to the type-0 and type-2 processes due to the induced correlation can be neglected (see Figure 5). As seeded FWM is an induced and cascaded effect emerging from the type-0 and type-2 processes, it should be proportional to the product of the square of both pump powers, i.e., $C \propto P_{TE}^2 P_{TM}^2$. These expected dependencies are exactly what can be observed in the left panels of Figure 5. When both TE and TM excitation powers are increased with a fixed power ratio ($P_{TM} = P_{TE}/4$, blue dots), both type-0 and type-2 processes show a quadratic scaling while the seeded FWM shows a quartic scaling. When only the TE pump power is increased with a fixed TM power ($P_{TM} = 110$ μW, black squares), TM type-0 FWM nearly remains unchanged (induced correlation contributions can be neglected), the type-2 FWM process behaves linearly, and the seeded process reveals a quadratic scaling. The right panels in Figure 5 show the respective CARs of different photon generation processes. In both cases (a fixed power ratio $P_{TM} = P_{TE}/4$ and a fixed TM power $P_{TM} = 110$ μW), the CARs of the type-0 and type-2 processes are always higher when the power ratio, rather than the TM power, is fixed. This is particularly evident in the low-power regime of the type-2 process. The reason is that the photons from the strong TM type-0 process are seen as noise in the context of the type-2 process. For the seeded process, a higher coincidence count in the fixed power ratio case leads to a quicker rise of the CAR, which reaches 1.5 at the highest available pump power.

We further looked at the power scaling of the coincidence counts from a different angle, i.e., by increasing the TM pump power while maintaining the TE pump power. We performed two sets of coincidence count measurements under the same exact conditions, except that the TE pump power in one measurement was around half of the other one – 440 and 200 μW, respectively. The ratio of generated photon counts at two different TE pump powers in the type-0, type-2, and seeded processes scaled linearly, quadratically, and quadratically with the power ratios, respectively. This was confirmed by the observation in **Figure 6**a, where the generation rate ratio extracted from the experimental

data (markers) was independent of the pump TM power, and showed good agreement with the theoretical values (solid lines). In terms of conversion efficiency (defined as coincidence counts/single counts) of the seeded FWM ($\propto P_{TM}P_{TE}$), the power of one pump field was kept constant while the power of the second one was increased, predicting a linear scaling behavior, whereas if the power of both pump fields is simultaneously increased with a constant power ratio, a quadratic scaling is expected. The experimental results in Figure 6b readily verify such theoretical predictions. The ratio converges to 5% at the maximum achievable power, which agrees well with the value indicated in Figure 4.

In conclusion, we demonstrate induced photon correlations through the interaction of two different spontaneous parametric processes. We show that sharing one common idler mode between the two nonlinear processes correlates the two signal photons belonging to different modes. We confirm this via temporal and power-dependent correlation measurements that showed a quartic behavior with pump powers, with a maximum induced ratio of 5%. Our integrated platform enables us to manipulate the dispersion of the two orthogonally polarized modes with very similar free spectral ranges in order to create and isolate the interaction between two different processes, which is very challenging to achieve in other nonresonant structures or with free space-based cavities. Our findings are important for the understanding of nondeterministic single photon sources.

Acknowledgements

The authors wish to acknowledge the following funding: Canada Research Chairs; Ministère de l'Économie, de la Science et de l'Innovation (MESI) Québec; Natural Sciences and Engineering Research Council of Canada (NSERC); Fonds de recherche du Québec—Nature et technologies (FRQNT) (B3655793); German federal ministry of education and research, Quantum Futur Program (PQuMAL); European Union's FP7 Programme (PIOF-GA-2013-625466); Australian Research Council (ARC) (DP150104327); Strategic Priority Research Program of the Chinese Academy of Sciences, under Grant No. XDB24030000; Royal Society Research Grants (RGS\R1\191426). R.M. is affiliated to 10 as an adjoint faculty.

Conflict of Interest

The authors declare no conflict of interest.

Keywords

correlated photon pairs, integrated devices, spontaneous four-wave mixing

Received: March 30, 2020
Revised: May 18, 2020
Published online: July 20, 2020

[1] P. Walther, K. J. Resch, T. Rudolph, E. Schenck, H. Weinfurter, V. Vedral, M. Aspelmeyer, A. Zeilinger, *Nature* **2005**, *434*, 169.
[2] I. Ali-Khan, C. J. Broadbent, J. C. Howell, *Phys. Rev. Lett.* **2007**, *98*, 060503.
[3] V. Giovannetti, S. Lloyd, L. Maccone, *Nat. Photonics* **2011**, *5*, 222.
[4] S. Tanzilli, H. Riedmatten, H. Tittel, H. Zbinden, P. Baldi, M. Micheli, D. B. Ostrowsky, N. Gisin, *Electron. Lett.* **2001**, *37*, 26.
[5] X. Zhang, Y. Zhang, C. Xiong, B. J. Eggleton, *J. Opt.* **2016**, *18*, 074016.
[6] C. Xiong, C. Monat, A. Clark, C. Grillet, G. D. Marshall, M. J. Steel, J. Li, L. O'Faolain, T. F. Krauss, J. G. Rarity, B. J. Eggleton, *Opt. Lett.* **2011**, *36*, 3413.
[7] J. E. Sharping, K. F. Lee, M. A. Foster, A. C. Turner, B. S. Schmidt, M. Lipson, A. L. Gaeta, P. Kumar, *Opt. Express* **2006**, *14*, 12388.
[8] M. Chen, N. C. Menicucci, O. Pfister, *Phys. Rev. Lett.* **2014**, *112*, 120505.
[9] Y. Cai, J. Roslund, G. Ferrini, F. Arzani, X. Xu, C. Fabre, N. Treps, *Nat. Commun.* **2017**, *8*, 15645.
[10] J. Roslund, R. M. Araujo, S. Jiang, C. Fabre, *Nat. Photonics* **2014**, *8*, 109.
[11] R. Kumar, J. R. Ong, M. Savanier, S. Mookherjea, *Nat. Commun.* **2014**, *5*, 5489.
[12] S. Yokoyama, R. Ukai, S. C. Armstrong, C. Sornphiphatphong, T. Kaji, S. Suzuki, J. Yoshikawa, H. Yonezawa, N. C. Menicucci, A. Furusawa, *Nat. Photonics* **2013**, *7*, 982.
[13] X. Wang, L. Chen, W. Li, H. Huang, C. Liu, C. Chen, Y. Luo, Z. Su, D. Wu, Z. Li, H. Lu, *Phys. Rev. Lett.* **2016**, *117*, 210502.
[14] C. Reimer, M. Kues, P. Roztocki, B. Wetzel, F. Grazioso, B. E. Little, S. T. Chu, T. Johnston, Y. Bromberg, L. Caspani, D. J. Moss, R. Morandotti, *Science* **2016**, *351*, 1176.
[15] J. Wang, S. Paesani, Y. Ding, R. Santagati, P. Skrzypczyk, A. Salavrakos, I. Tura, R. Augusiak, L. Mančinska, D. Bacco, D. Bonneau, J. W. Silverstone, Q. Gong, A. Acin, K. Rottwitt, L. K. Oxenlowe, J. L. O'Brien, A. Laing, M. G. Thompson, *Science* **2018**, *360*, 285.
[16] P. Imany, J. A. Villegas, O. D. Odele, K. Han, D. E. Leaird, J. M. Lukens, P. Lougovski, M. Qi, A. M. Weiner, *Opt. Express* **2018**, *26*, 1825.
[17] M. Kues, C. Reimer, P. Roztocki, L. R. Cortés, S. Sciara, B. Wetzel, Y. Zhang, A. Cino, S. T. Chu, B. E. Little, D. J. Moss, L. Caspani, J. Azaña, R. Morandotti, *Nature* **2017**, *546*, 622.
[18] J. T. Barreiro, N. K. Langford, N. A. Peters, P. G. Kwiat, *Phys. Rev. Lett.* **2005**, *95*, 260501.
[19] C. Reimer, P. Roztocki, S. Sciara, M. Islam, L. Cortes, Y. Zhang, B. Fischer, S. Loranger, R. Kashyap, A. Cinio, S. Chu, B. Little, D. Moss, L. Caspani, W. Munro, J. Azaña, M. Kues, R. Morandotti, *Nat. Phys.* **2018**, *1*, 148.
[20] M. Malik, M. Erhard, M. Huber, M. Krenn, R. Fickler, A. Zeilinger, *Nat. Photonics* **2016**, *10*, 248.
[21] M. Erhard, M. Malik, M. Krenn, A. Zeilinger, *Nat. Photonics* **2018**, *12*, 759.
[22] S. Dong, X. Yao, W. Zhang, S. Chen, W. Zhang, L. You, Z. Wang, Y. Huang, *ACS Photonics* **2017**, *4*, 746.
[23] A. Hochrainer, M. Lahiri, R. Lapkiewicz, G. B. Lemos, A. Zeilinger, *Optica* **2017**, *4*, 341.
[24] L. J. Wang, X. Y. Zou, L. Mandel, *Phys. Rev. A* **1991**, *44*, 4614.
[25] C. Reimer, M. Kues, L. Caspani, B. Wetzel, P. Roztocki, M. Clerici, Y. Jestin, M. Ferrera, M. Peccianti, A. Pasquazi, B. E. Little, S. T. Chu, D. J. Moss, R. Morandotti, *Nat. Commun.* **2015**, *6*, 8236.
[26] M. Kues, C. Reimer, J. M. Lukens, W. J. Munro, A. M. Weiner, D. J. Moss, R. Morandotti, *Nat. Photonics* **2019**, *13*, 170.
[27] L. Caspani, C. Xiong, B. J. Eggleton, D. Bajoni, M. Liscidini, M. Galli, R. Morandotti, D. J. Moss, *Light: Sci. Appl.* **2017**, *6*, e17100.
[28] L. Caspani, C. Reimer, M. Kues, P. Roztocki, M. Clerici, B. Wetzel, Y. Jestin, M. Ferrera, M. Peccianti, A. Pasquazi, L. Razzari, B. E. Little, S. T. Chu, D. J. Moss, R. Morandotti, *Nanophotonics* **2016**, *5*, 351.
[29] D. J. Moss, R. Morandotti, A. L. Gaeta, M. Lipson, *Nat. Photonics* **2013**, *7*, 597.
[30] P. Roztocki, S. Sciara, C. Reimer, L. Cortes, Y. Zhang, B. Wetzel, M. Islam, B. Fischer, A. Cino, S. Chu, B. Little, D. Moss, L. Caspani, J. Azaña, M. Kues, R. Morandotti, *J. Lightwave Technol.* **2018**, *37*, 338.

[31] A. Pasquazi, M. Peccianti, L. Razzari, D. J. Moss, S. Coen, M. Erkintalo, Y. K. Chembo, T. Hansson, S. Wabnitz, P. Del'Haye, X. Xue, A. M. Weiner, R. Morandotti, *Phys. Rep.* **2018**, *729*, 1.
[32] L. Helt, L. Marco, J. Sipe, *J. Opt. Soc. Am. B* **2012**, *29*, 2199.
[33] Z. Ou, Y. Lu, *Phys. Rev. Lett.* **1999**, *83*, 2556.
[34] M. Förtsch, J. U. Fürst, C. Wittmann, D. Strekalov, A. Aiello, M. V. Chekhova, C. Silberhorn, G. Leuchs, C. Marquardt, *Nat. Commun.* **2013**, *4*, 1818.
[35] D. J. Kane, R. Trebino, *IEEE J. Quantum Electron.* **1993**, *29*, 571.
[36] E. K. Tien, X. Sang, F. Qing, Q. Song, O. Boyraz, *Appl. Phys. Lett.* **2009**, *95*, 051101.